12

PHASED ARRAYS

Chapter 3 covers the basics of phased arrays. We place phase shifters or time-delay networks on every element or a combination of these in a feed network to shift the beam direction. In this chapter we discuss the particular problems of phased arrays when we consider the effects of phase shifters and architecture of the feed network. In Chapter 4 we discuss array pattern synthesis using direct methods and array characteristics of those that sample aperture distributions. We do not repeat those topics in this chapter.

The pattern properties desired determine the number of array elements and their layout, from which we calculate gain as discussed in Section 3-12. To prevent grating lobes (Sections 3-5 and 3-8), we must place an element approximately every $\lambda/2$ for an array that scans to 90°. Of course, if we limit scan, we may place elements farther apart. By using a uniform linear aperture beamwidth approximation to a line array, its beamwidth is 100 (HPBW factor)/N_x in degrees for the general amplitude distribution when elements are spaced $\lambda/2$. We initially ignore the HPBW factor and assume a uniform distribution (minimum beamwidth). Given the beamwidth in the principal planes, θ_x and θ_y, the number of elements in the array is

$$N = N_x N_y = \frac{10{,}000}{\theta_x \theta_y} \tag{12-1}$$

When we use a tapered distribution to lower sidelobes, the required number of elements increases by the HPBW factors in the two planes. Section 3-12 showed that array gain is limited by its area for closely spaced elements. The area of $\lambda/2$ spaced elements is $\lambda^2/4$, which relates gain to the number of elements by effective area:

$$\text{gain} = \pi N \tag{12-2}$$

This assigns an effective gain of π to each element. When we scan the beam, the effective area (length in the scan plane) drops by cos θ_0, which causes gain to drop

Modern Antenna Design, Second Edition, By Thomas A. Milligan

and beamwidth to broaden:

$$\text{gain} = \pi N \cos\theta_0 \quad \text{and} \quad \theta_x(\text{scanned}) = \frac{\theta_x}{\cos\theta_0} \tag{12-3}$$

Because the gain drops by $\cos\theta_0$ as the beam scans, it leads to the idea of an element pattern:

$$E_e(\theta) = \sqrt{\cos\theta} \tag{12-4}$$

The element pattern alters the array factor pattern as the element is scanned. In general, narrow beamwidth elements greatly alter the pattern when the array factor scans across the element pattern, and it limits the practical scan range. To scan to wide angles, we need broad-beamwidth array elements.

Aperture theory uses a Huygens source along the array with a pattern given by

$$E(\theta) = \cos^2\frac{\theta}{2}$$

a function with values almost identical to those of the ideal element pattern [Eq. (12-4)]. The Huygens source is the combination of electric and magnetic incremental sources whose ratio equals the free-space impedance $\eta = 376.73$. A Huygens source array element impedance matched at broadside has a resistance η. Scanning the array in the E-plane foreshortens the electric field by $\cos\theta_0$, which reduces the resistance by the same factor:

$$\eta_E = \frac{E\cos\theta_0}{H} = \eta\cos\theta_0 \tag{12-5}$$

In the same manner the magnetic field is foreshortened for scan in the H-plane. The scan resistance becomes

$$\eta_H = \frac{E}{H\cos\theta_0} = \frac{\eta}{\cos\theta_0} \tag{12-6}$$

Equations (12-5) and (12-6) predict the general nature of array element impedance when it scans. E-plane scanning reduces input resistance while H-plane scanning increases resistance, a consequence of the infinite current sheet model [1,2]. A finite array has an impedance response generally similar to Eqs. (12-5) and (12-6) but dependent on element position. General scanning has a resistance response relative to the broadside value R_0 given by

$$\eta(\theta,\phi) = \frac{(1-\sin^2\theta\cos^2\phi)R_0}{\cos\theta} \tag{12-7}$$

In Section 3-9 we discuss how to use self- and mutual impedance to find the scan impedance for a finite array, and in Section 11-7 we discuss the interaction of the element impedance with the feed network.

12-1 FIXED PHASE SHIFTERS (PHASERS)

In a phased array every antenna element is connected to a phase shifter or time-delay network. We scan the beam by commanding every network to compensate for the extra time it takes the signal to propagate to a plane normal to the beam direction. Phase shifters operate in terms of a single frequency in a modulo 2π radians fashion

to compensate for the kd_i phase distance to the reference plane for the ith element, where d_i is the distance and $k = 2\pi/\lambda$.

The ideal phased array uses switched time-delay networks because the beam remains at a fixed direction as frequency changes. We make time-delay networks by varying lengths of transmission lines. In large phased arrays that use fixed phase differences instead of time-delay networks, we use time-delay networks near the input to limit the size of the phase-shift-controlled subarrays to increase bandwidth. Switching the length of a transmission line changes the insertion loss, and the switched time delay modulates the element amplitudes. We must add amplitude control in the time delay to compensate for the varying insertion loss to maintain the design aperture distribution. Another approach modulates a laser beam with RF signal, uses low-loss fiber optics to switch time delays, and detects the optical signal to recover the RF before transmission. Fortunately, the losses are so low when switching fiber optics that amplitude control is unnecessary. Unfortunately, the modulator losses must be overcome to make this approach useful.

Some phase shifters (also called *phasers*) are made by switching short transmission-line sections, but the modulo nature of their phase shift limits bandwidth. The most common feed architecture has equal path lengths from the single input to the multiple radiating elements, and the equal path lengths of the corporate feed maintain the arrays broadside pointing when frequency shifts. If we scan a beam by setting phase shifters based on frequency and scan angle, the beam will scan toward broadside as frequency increases. The amount of angular beam shift is independent of the array size, as given by Eq. (3-14). For a planar surface array with its normal along the z-axis with beam scanned to θ_0, measured from the normal vector, changing frequency shifts the beam $\Delta\theta$:

$$\Delta\theta = \frac{f_2 - f_1}{f_2} \tan\left(\frac{\pi}{2} - \theta_0\right) \tag{12-8}$$

where f_1 and f_2 are the two frequencies. Figure 12-1 shows the beam scanning due to a 5% change in frequency. Figure 12-1 was drawn for a particular array, but the

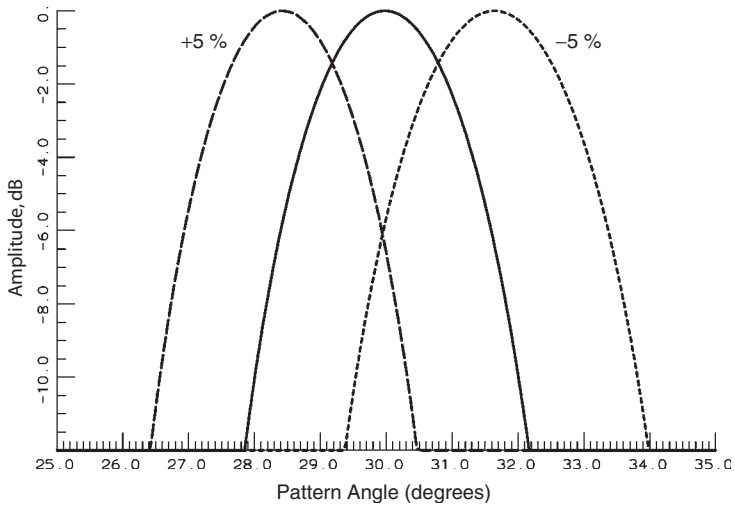

FIGURE 12-1 Scan of array with fixed phase shifters for 5% frequency shift scanned to 30°.

beam shift is independent of array size because array length affects only beamwidth. Larger arrays shift their beams the same amount as do short arrays. Only when we define bandwidth in terms of a factional part of the beamwidth do shorter arrays have greater bandwidth.

We can use frequency shift to scan a linear array beam direction. The array must be series-fed similar to waveguide slots, where a single line feeds the array by having each element coupling a portion of the remaining power traveling down the transmission line. Figure 12-2 shows the nature of the series feed in terms of slot radiators that can be replaced by any antenna element. We load the transmission line after the last element. We use this feeding arrangement for waveguide-fed slot arrays, except that we use straight sections of waveguide to reduce beam scanning as frequency changes. In this application we add a meander to increase the electrical length between elements. Given element-to-element spacing d and a length along the meander s, in general made from a waveguide with relative propagation constant P, we find the phasing equation of the radiated wave:

$$kd\cos\theta + 2\pi N = Pks + (-\pi) \quad \text{for} \quad P = \frac{\lambda}{\lambda_g} = \sqrt{1 - \left(\frac{\lambda}{\lambda_c}\right)^2} \tag{12-9}$$

The $-\pi$ term occurs when we have alternating phases on the elements, such as alternating slots. For coax line we use the dielectric constant for $P = \sqrt{\varepsilon_r}$. For a given N we solve for the meander length s:

$$\frac{s}{\lambda} = \frac{1}{P}\left[\frac{d}{\lambda}\cos\theta_M + \left(N + \frac{1}{2}\right)\right] \tag{12-10}$$

The $\frac{1}{2}$ term is included for alternating phases on the elements. Larger values of N increase the beam direction frequency slope:

$$f\frac{d\theta}{df} = \begin{cases} -\left[\dfrac{s}{d}\left(\dfrac{\lambda}{\lambda_c}\right)^2\dfrac{1}{P} + \dfrac{\left(N+\frac{1}{2}\right)\lambda}{d}\right]\dfrac{1}{\sin\theta}(\text{rad}) & \text{waveguide} \\ -\left[\dfrac{s}{d} + \dfrac{\left(N+\frac{1}{2}\right)\lambda}{d}\right]\dfrac{1}{\sin\theta}(\text{rad}) & \text{coax} \end{cases} \tag{12-11}$$

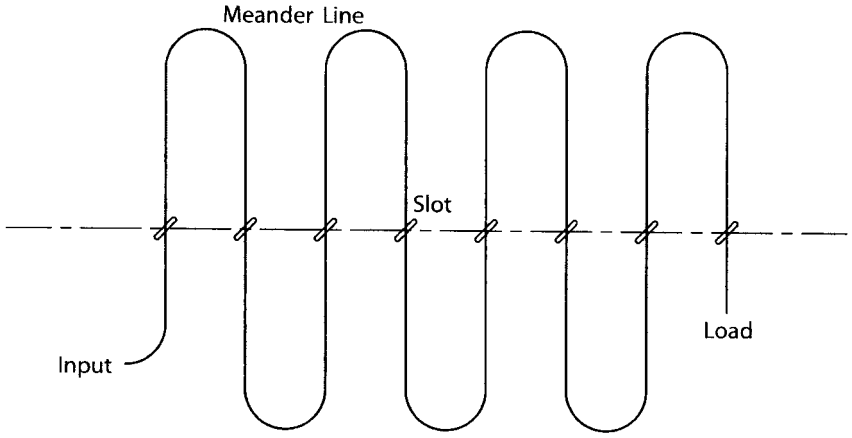

FIGURE 12-2 Frequency scanning array using the meander line between antennas.

Example For a coaxial feeder using $N = 8$ and a spacing $D/\lambda = 0.6$, find the phase slope when $\theta_M = 90^\circ$ and the elements do not have alternating phases.

We substitute these values into Eq. (12-11*b*):

$$\Delta\theta = -\frac{\Delta f}{f}\frac{8}{0.6} = -13.33\frac{\Delta f}{f}(\text{rad}) = -764\frac{\Delta f}{f}(\text{deg})$$

To shift the beam 30°, we change frequency by 3.93%.

Phasers have been designed using high-speed diode switches and lower-speed ferrite devices. The diode (or FET) switches enable rapid scan but have high loss compared to ferrite phasers. The switches redirect the RF path through different lengths of transmission lines and lead to digital phasers. A digital phase shifter has quantized values: 180°, 90°, 45°, 22.5°, and so on, at a particular frequency. Each phaser bit directs the signal through one of two paths, each containing two diode switches, whose nearly equal losses reduce amplitude modulation. But we must design carefully for impedance match in both states to prevent amplitude modulation. Each bit adds significant transmission loss due to the diode switches, and unfortunately, all bits are in series. Adding bits gives better control but increases loss.

The design of transmit/receive (T/R) modules eliminates phaser loss system impacts. If the antenna both transmits and receives signals, such as radar, we add two paths through the module and rely on the nonreciprocal nature of amplifiers to separate the channels. Of course, if the antenna does only one function, we eliminate its path. When transmitting, a final amplifier produces almost all the power when its output is connected to the antenna. The phaser operates on the drive signal and the amplifier overcomes the phaser loss. In the receive channel the signal first passes through a low-noise amplifier (LNA) connected to each antenna element. Section 1-15 shows that a LNA with sufficient gain overcomes the loss of networks with high loss (and noise figure) that follow in the receiver chain. The amplifier overcomes the phaser loss that follows it.

Ferrite phase shifters operate along a magnetic hysteresis loop and it is latched at a zero magnetic drive point for a given phase shift. This requires drive magnetic fields to cycle it along the loop to produce the desired value, but operate only when changing phase. For arbitrary phase shift the ferrite must be demagnetized before changing to a new state. An alternative design digitizes the ferrite cores by using shorter cores and pulse magnetic fields developed by current pulses through a wire that threads through the center of the core to latch it at the two opposite points along the hysteresis loop. We mount the ferrite toroidal cores in a waveguide and vary the lengths to alter the phase shift. The phase shift depends on the direction of the wave through the ferrite phaser. It is nonreciprocal, and in radar all phasers must be reset between transmittal and receipt of pulses. Reciprocal Faraday rotation phasers convert the input signal to circular polarization in the waveguide by using a quarter-wave plate tilted at 45° along the axis of a circular waveguide relative to the input linear polarization. The input wave divides into two signals at the quarter-wave plate, which retards or advances the two signals relative to a waveguide without the plate until their phase difference is 90°. The wave exits as circular polarized. The magnetized ferrite alters the phase of the CP wave independent of direction. On the output another quarter-wave plate converts the wave to a linearly polarized wave. Although ferrite phasers are analog devices

capable of any phase shift, the drive currents are controlled by digital commands and our designs end up having quantized values.

12-2 QUANTIZATION LOBES

Quantization of the phase shifters produces extra sidelobes for scans near broadside. We apply a linear-phase slope across the face to scan an array, and the distance between phase changes is large for scans near broadside because the phase slope is shallow. These widely spaced phase changes produce grating lobes. Given the scan angle θ_0 for an array with M bits in the phase shifters, the quantization lobes are evenly spaced in sin θ-space:

$$\theta_q = \sin^{-1}[\sin\theta_0(1 \pm N \cdot 2^M)] \tag{12-12}$$

The quantization lobes occur at every integer N until θ_q leaves visible space. Figure 12-3 gives the pattern of a 128-element linear array with amplitudes from sampling a 30-dB Taylor distribution scanned to 1° and illustrating quantization lobes. The inner two quantization lobes can be found from Eq. (12-12) for $N = 1$:

$$\theta_q(-1) = \sin^{-1}[\sin(1^\circ)(1-8)] = -7.02^\circ$$
$$\theta_q(1) = \sin^{-1}[\sin(1^\circ)(1+8)] = 9.04^\circ$$

Figure 12-4 shows how the quantization lobes appear at greater angles as the array scan increases, but the sidelobe levels are approximately the same in Figures 12-3 and 12-4. Figure 12-5 illustrates the effect of adding another bit to the phase shifters. The quantization lobes move out in angle and reduce in level for additional bits in the phase shifters. These sidelobes have predictable levels. We use the peak sawtooth phase error due to quantization $\beta = \pi/2^M$, and the lobe voltage amplitude is given by

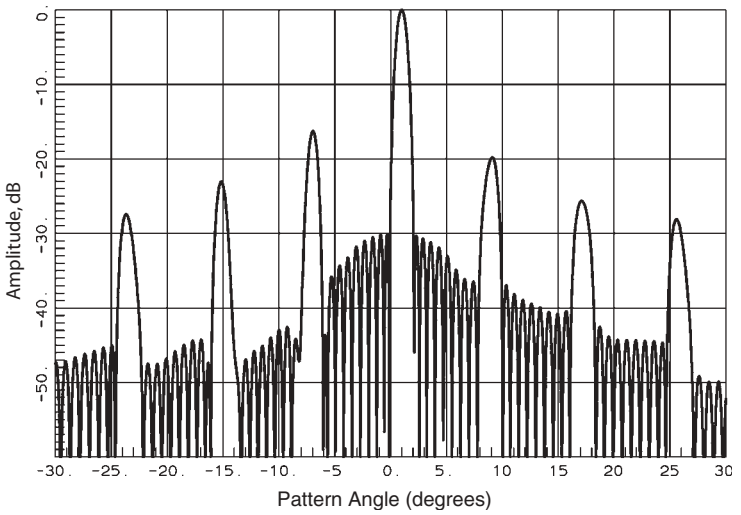

FIGURE 12-3 Quantization lobes of a 128-element line array (30-dB Taylor distribution) with 3-bit phase shifters scanned to 1°.

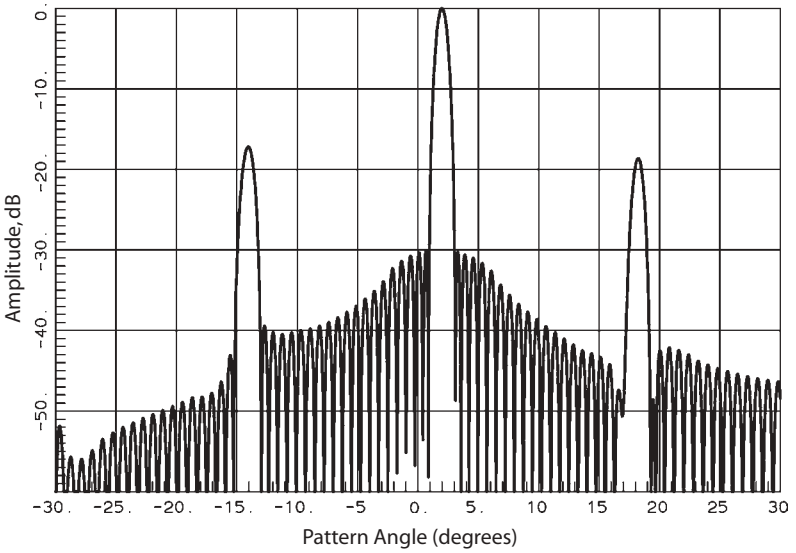

FIGURE 12-4 Quantization lobes of a 128-element line array (30-dB Taylor distribution) with 3-bit phase shifters scanned to 2°.

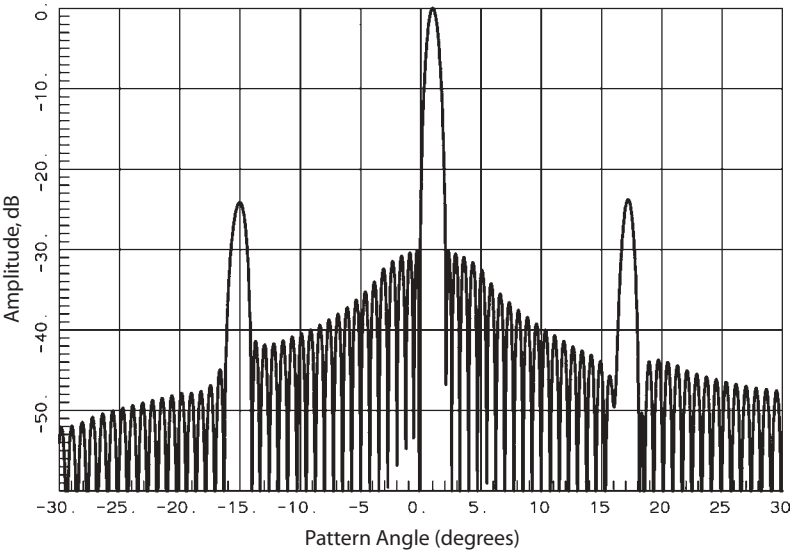

FIGURE 12-5 Quantization lobes of a 128-element line array (30-dB Taylor distribution) with 4-bit phase shifters scanned to 1°.

$\text{sinc}(\beta \pm N\pi)$ for a uniform amplitude array. $N = 0$ is the main beam, which gives the quantization loss due to phase shifters. Table 12-1 lists the main-beam loss and quantization lobe (QL) amplitudes versus the number of bits M in the phase shifters for a positive scan. The negative QL appear on the opposite of the scan. There are no QL values for a scan of zero. We can solve Eq. (12-12) for the scan angle that places

TABLE 12-1 Quantization Sidelobe Levels and Scan of Last QL for a Phased Array

Phase Bits, M	Main-Beam Loss (dB)	−2 QL (dB)	−1 QL (dB)	+1 QL (dB)	+2 QL (dB)	Scan Angle of Last QL	Scan Increment Ratio of BW
2	0.91	17.8	10.4	14.9	20.0	19.47	0.243
3	0.22	23.7	17.1	19.3	24.8	8.21	0.121
4	0.056	29.9	23.6	24.7	30.4	3.82	0.0607
5	0.014	36.0	29.8	30.4	36.3	1.85	0.0304
6	0.003	48.1	42.1	42.2	42.2	0.91	0.0152

the first quantization lobe at -90° and eliminates them for all higher scan angles:

$$\theta_0 = \sin^{-1} \frac{1}{2^M - 1} \tag{12-13}$$

Table 12-1 lists the scan angle that places the first quantization lobe at -90°. The number of phase bits limits the scan increments given as a ratio of the 3-dB beamwidth θ_3 [3]. Table 12-1 lists this ratio:

$$\frac{\theta_{\text{incr}}}{\theta_3} = \frac{1}{2^M(1.029)} \tag{12-14}$$

12-3 ARRAY ERRORS [4; 5; 6, pp. 393–399]

Phase arrays contain random errors that lower gain and increase sidelobe levels. We assume a Gaussian distribution for random amplitude and phase errors with zero mean and variances of $\overline{\Delta}^2$ (volts)^2 for amplitude and $\overline{\delta}^2$(radians)^2 for phase. Although quantization of phase shifters is a systematic error, we can assign a variance to it. The peak error of a quantized phase shifter is $\pi/2^M$ (radians). We calculate the equivalent Gaussian distribution variance of this triangular error distribution:

$$\delta_Q^2 = \frac{\pi^2}{3(2^{2M})} \qquad \text{rad}^2 \tag{12-15}$$

We add this variance to the phase term. Array element failure lowers gain and raises sidelobes. P_e is the probability of survival for each element in the array. The advantage of an array is the graceful degradation of the pattern as elements fail and no single failure shuts down the system. The gain reduction is given by

$$\frac{G}{G_0} = \frac{P_e}{1 + \overline{\Delta}^2 + \overline{\delta}^2} \tag{12-16}$$

We find the efficiency of an array in the same manner as amplitude taper efficiency of a continuous distribution (Section 4-1) by replacing the integrals with summations and using constant phase for the voltage (current) amplitudes a_i of the elements:

$$\eta_a = \frac{\left(\sum_{i=1}^{N} |a_i|\right)^2}{N \sum_{i=1}^{N} |a_i|^2} \tag{12-17}$$

The average sidelobe level σ_s^2 (volts)^2 is related to the beam peak provided that we consider the far sidelobes:

$$\sigma_s^2 = \frac{(1 - P_e) + \overline{\Delta}^2 + \overline{\delta}^2}{P_e N \eta_a} \tag{12-18}$$

Equation (12-18) shows that to achieve low sidelobes, we must control the amplitude and phase errors of elements in an array and that increasing the number of elements decreases the requirements on feeding errors. Sidelobes follow a Rayleigh distribution, and the probability that a sidelobe exceeds a level v_0^2 (volts)^2 is given by

$$P(v > v_0) = e^{-v_0^2/\sigma_s^2} \tag{12-19}$$

We solve Eq. (12-18) for requirements on arrays to achieve average sidelobes:

$$\text{phase error variance } \overline{\delta}^2 = \sigma_s^2 N \eta_a - (1 - P_e + \overline{\Delta}^2)$$

$$\text{amplitude error variance } \overline{\Delta}^2 = \sigma_s^2 P_e N \eta_a - \overline{\delta}^2 - 1 + P_e$$

$$\text{element survivability } P_e = \frac{1 + \overline{\Delta}^2 + \overline{\delta}^2}{\sigma_s^2 N \eta_a + 1}$$

$$\text{number of elements } N = \frac{1 - P_e + \overline{\Delta}^2 + \overline{\delta}^2}{P_e \sigma_s^2 \eta_a}$$

If we substitute Eq. (12-14) into Eq. (12-18), we find the average sidelobe level due to phase quantization:

$$\text{SL(dB)} = 10 \log \left(\frac{\pi^2}{3(2^{2M})} \right) - 10 \log(N) - 10 \log(\eta_a) \tag{12-20}$$

Table 12-2 gives the first term of Eq. (12-20).

Example Given a 64-element array with amplitudes found by sampling a 30-dB Taylor distribution, find the RMS sidelobes versus phase quantization.

TABLE 12-2 Average Sidelobe Factor Due to Phase Quantization Normalized to the Number of Elements and Array Efficiency

Number of Bits	Sidelobe Factor (dB)
1	−0.9
2	−6.9
3	−12.9
4	−18.9
5	−24.9
6	−31.0
7	−37.0

The efficiency of the Taylor distribution is 0.66 dB, from Table 4-5. The element number factor 10 log(N) is 18.06 dB.

$$\text{SL(dB)} = \begin{cases} -12.9 - 18.06 + 0.66 = -30.3 & \text{for 3 bits} \\ -18.9 - 18.06 + 0.66 = -36.3 & \text{for 4 bits} \end{cases}$$

Of course, the distribution will determine the sidelobe levels in the pattern. With only 3 bits, we can expect the peak sidelobes to rise above 30 dB. Quantization lobes exceed these levels for scan angles close to broadside. This example and Eq. (12-20) show that the sidelobe level is proportional to 10 log(N).

12-4 NONUNIFORM AND RANDOM ELEMENT EXISTENCE ARRAYS [4]

12-4.1 Linear Space Tapered Array

Array synthesis discussed in Chapter 4 uses uniformly spaced elements. For arrays along a line, we can analyze them by the Schelkunoff unit circle. These arrays control the sidelobe level by tapering element amplitudes: high in the center and tapered at both ends. We can design planar arrays by sampling aperture distributions, such as the circular Taylor distribution for arrays confined to circles or hexagons. These taper element amplitudes as well. An alternative approach is to taper the spacing between elements fed with uniform amplitude so that the average follows an aperture distribution. When we sample an aperture distribution, we have each element sample a length along the distribution equal to the element spacing. We either find the element amplitude by point sampling the distribution at the element location or we integrate the aperture distribution plus and minus the half-element spacing. Integrating along the distribution produces a better match between the pattern of array and the aperture distribution, but for large arrays we notice little difference between methods. For a nonuniformly spaced array we assign half spacing on each side of the element for integration along the sampled aperture distribution. Because we feed all elements with the same amplitude, we space elements so that the integral of the aperture distribution over each spacing interval is the same for each element.

Figure 12-6*a* illustrates sampling the aperture distribution with an array so that the area under the region assigned to each element is the same. To find element locations, we start by generating a table of the cumulative distribution. We calculate this by integrating the normalized length distribution from the start at -0.5 to a given point x:

$$I(x) = \int_{-0.5}^{x} E(x)\,dx \tag{12-21}$$

We divide this cumulative distribution into equal-length intervals along the ordinate as shown in Figure 12-6*c*, equal to the number of elements in the array. We locate the position of the element by projecting the center of each interval to the abscissa. Instead of using a graphical technique, we calculate a cubic spline with $I(x)$ as the independent variable normalized to 1 and x as the dependent variable. We evaluate the spline at $(i - 0.5)/N$ to find element location x_i. So far we have only found the relative element location normalized to an array length of 1. We have two choices. We can choose the spacing of the closest elements because our planned elements have

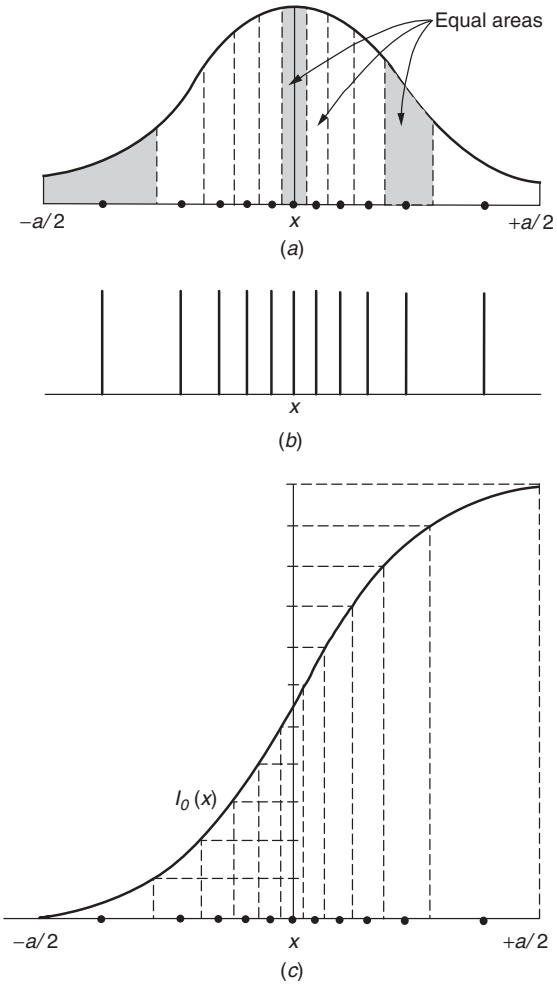

FIGURE 12-6 Deterministic density taper for a line array: (*a*) amplitude taper divided in equal areas; (*b*) location of elements; (*c*) cumulative distribution equally divided along ordinate. (From [4], Fig. 6.2, © 1969 McGraw-Hill.)

a given size and we need to limit mutual coupling. This scales the location of all elements and determines the effective array length. In the second choice we design to a given beamwidth that determines the total array length by considering the half-power beamwidth factor of the distribution sampled. In this case we scale element locations by this length.

A 32-element space tapered array was designed for a 30-dB Taylor linear distribution. Figure 12-7 gives the relative element locations along the line, and Table 12-3 lists element locations when the center element spacing is 0.45λ. Figure 12-8 shows the calculated pattern of this array and another designed with 24 elements, both using elements with 90° beamwidths. The 24-element array has a larger beamwidth because it is shorter. These two patterns show that increasing the number of elements improves the ability of the array to realize the aperture distribution pattern. With so

FIGURE 12-7 Locations of a 32-element space tapered line array for 30-dB Taylor distribution.

TABLE 12-3 Space-Tapered 32-Element Array for 30-dB Taylor Linear Distribution

Element	Position	Element	Position
32, 1	±10.288	24, 9	±3.552
31, 2	±8.798	23, 10	±3.036
30, 3	±7.649	22, 11	±2.539
29, 4	±6.739	21, 12	±2.059
28, 5	±5.971	20, 13	±1.590
27, 6	±5.291	19, 14	±1.130
26, 7	±4.671	18, 15	±0.676
25, 8	±4.095	17, 16	±0.225

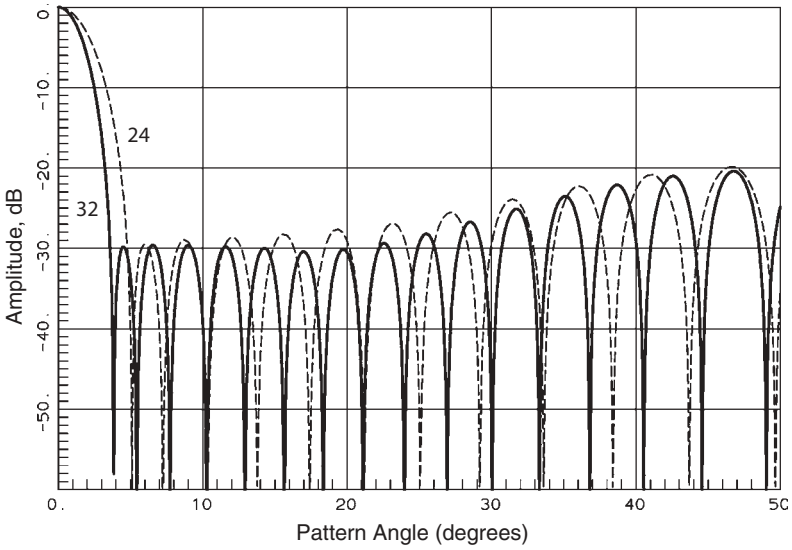

FIGURE 12-8 Pattern of space tapered arrays using 90° beamwidth elements: 32 elements (solid); 24 elements (dashed).

few elements the far sidelobes rise because we narrow the beamwidth relative to a uniformly spaced array that does not radiate grating lobes. The nonuniformly spaced array will not produce lobes at the same amplitude of the main beam, grating lobes of the uniformly spaced array, but spreads the power in these lobes among all far sidelobes.

12-4.2 Circular Space Tapered Array

Space tapered arrays can be designed for circular aperture distributions by evenly spacing array elements in rings [7]. We start by designing a circular aperture distribution,

such as the Taylor distribution (Sections 4-18 and 4-19). We choose a distribution for the spacing of elements in the rings as a function of radius, $d_e(r)$: generally wider near the edge, to match the circular aperture distribution. A table of the cumulative distribution is found by integrating the voltage distribution times the element spacing function $d_e(r)$ from zero to a given radius r:

$$I(r) = \int_0^r d_e(\rho) E(\rho)\, d\rho \tag{12-22}$$

Figure 12-9 shows the division of the cumulative distribution into 10 rings for a 30-dB circular Taylor distribution where the element spacing $d_e(r)$ is a linear function from 0.66λ to 1.4λ from the center to the edge. A ring is located in the center of each region along the radius where the maximum aperture radius is 8.5λ. We space the elements evenly around each ring of radius r_i:

$$N_i = \frac{2\pi r_i}{d_e(r_i)} \tag{12-23}$$

Because N_i must be integers, the radial element spacing only approximately satisfies the $d_e(r)$ distribution when we design small arrays. Table 12-4 lists the parameters of a 10-ring design.

The diagram of the element positions (Figure 12-10) shows the increasing element spacing as radius increases. The combination of Figures 12-9 and 12-10 illustrates the nearly even ring spacing, due to a design with increasing element spacing with radius. Figure 12-11 plots the pattern response and shows the nearly equal sidelobe response for the first few sidelobes. Adding rings improves the match between the aperture distribution and the space tapered array radiation patterns.

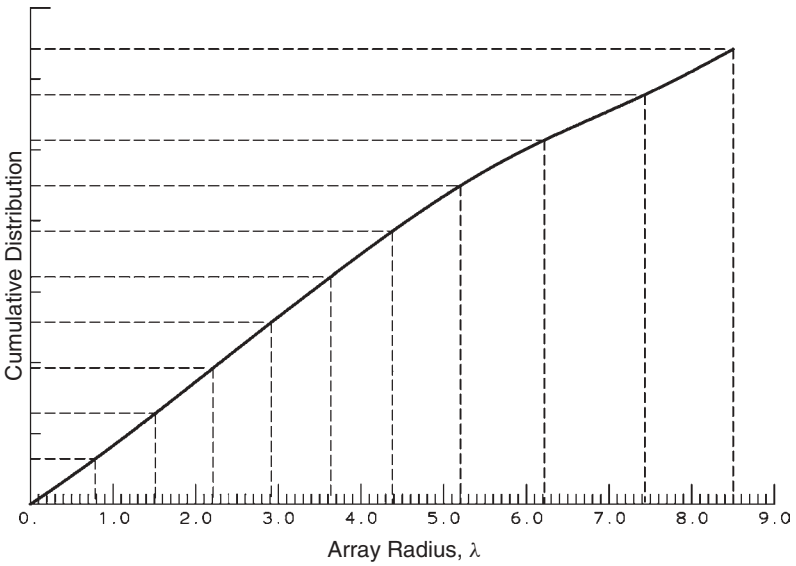

FIGURE 12-9 Cumulative aperture distribution of a 10-ring space tapered (30-dB Taylor distribution) ring array with linear taper on the element spacing from 0.66λ to 1.4λ.

TABLE 12-4 Design of a 10-Ring (223 Elements) Space Tapered Array for 30-dB Circular Taylor Distribution with Linearly Tapered Radial Spacing from 0.66λ to 1.4λ

Ring	Radius	N_i	d_e	Ring	Radius	N_i	d_e
1	0.403	4	0.695	6	4.004	25	1.009
2	1.155	10	0.761	7	4.779	28	1.076
3	1.864	14	0.822	8	5.677	31	1.154
4	2.562	18	0.883	9	6.826	34	1.254
5	3.272	22	0.945	10	7.989	37	1.356

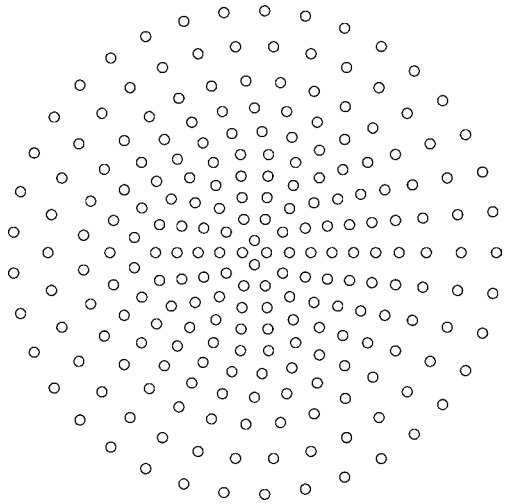

FIGURE 12-10 Layout of a 223-element ring array for 30-dB circular Taylor distribution with 10 rings.

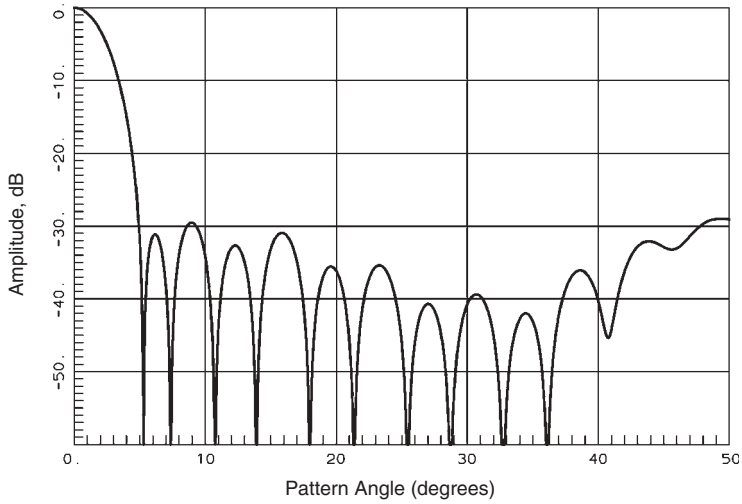

FIGURE 12-11 Pattern of a 223-element space tapered ring array with 90° beamwidth elements.

12-4.3 Statistically Thinned Array [8]

Low sidelobe patterns can be obtained from uniform-amplitude fed arrays by thinning a uniformly spaced array statistically. Each element has a random chance of existence, determined by using the aperture distribution as the probability density function. In this method we lay out a uniformly spaced array and use a random number generator output times the desired aperture distribution to determine whether to include each element. We multiply the product of the random number [0,1] by the aperture distribution [0,1] and by a scale factor k to scale to the level of thinning. We call $k = 1$ natural thinning because the process removes about half the elements. When the random number is higher than the product of k times the aperture distribution, the element is removed, and therefore a lower k produces greater thinning.

Thinning reduces gain by the ratio of the remaining elements to the initial total, but array size determines beamwidth. We obtain patterns determined by aperture extent but with reduced gain. The number of elements determines the average sidelobe level at 10 $\log(N)$ dB. Provided that we use sufficient elements, the near-in sidelobes will follow the aperture distribution, but the far-out sidelobes rise to the average level. For initially large arrays, 90% thinning is reasonable. A convenient method in a computer program is to mark elements for removal and report on the remaining element number so that the algorithm can be repeated after adjusting k until the desired number is achieved before actual removal. We obtain a different number of elements with the same k because of the variability of the random number generator.

To show the method we pick a hexagon array with 0.66λ element spacing first confined to a radius $= 8.7\lambda$. A 30-dB circular Taylor distribution used as the probability density and $k = 1$ produced an array with 337 elements starting from an array with 637 elements inside the circle. Figure 12-12 shows the layout of the remaining elements. The low aperture distribution near the rim removed many of the outer elements while

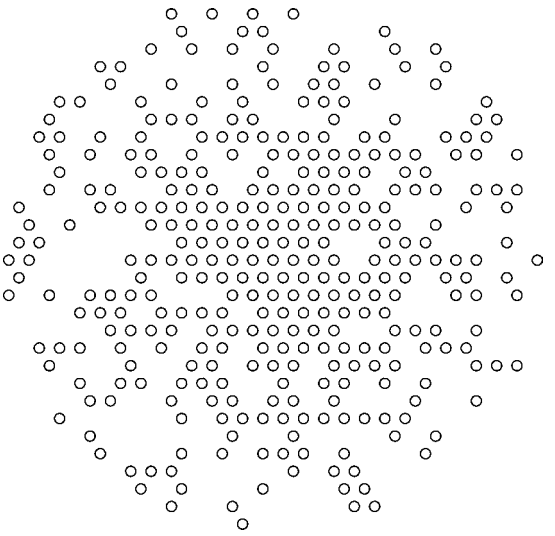

FIGURE 12-12 Layout of a 337-element statistically tapered array for 30-dB circular Taylor distribution.

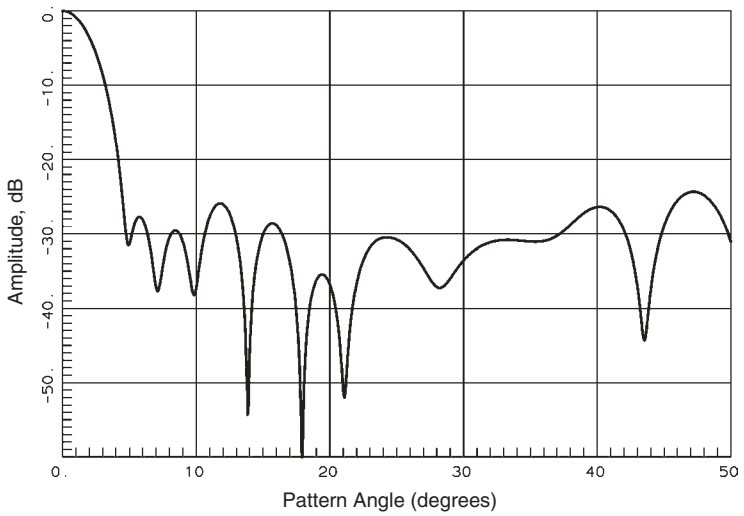

FIGURE 12-13 Pattern of a 337-element statistically tapered array for 30-dB circular Taylor distribution using 90° beamwidth elements.

most of the inner elements remain. Figure 12-13 plots the pattern response of this array when 90° beamwidth elements are used in the array.

12-5 ARRAY ELEMENT PATTERN

When we insert an antenna element into an array, its effective pattern changes. Throughout the book we have shown that the pattern of isolated elements change when we mount them on finite ground planes. An antenna mounted over a ground plane excites currents on it that radiate and contribute to the pattern. We place many antennas near each other in a phased array. Radiation from one antenna excites currents on its neighbors, and the sum of these currents radiates a pattern different from that of the isolated element. If we want to apply pattern multiplication between the array factor and the element pattern, we need to modify the element pattern to include the radiation from the current excited on its neighbors. This is a simplifying assumption because in the final configuration the array will be mounted on a finite ground plane, and not all elements will be surrounded by the same configuration of elements. Each element will have a different pattern, but to first order we use the array element pattern.

We could assume current basis functions on the elements and on the nearby structure and use an integral equation method to solve for the coefficients of these basis functions (moment method). The final pattern calculated would be found from a weighted sum of currents. By increasing the number of basis functions, the calculation converges to the measured result (within measurement error). We simplify the problem by assuming an infinite mounting structure to eliminate edge effects that eliminate the basis functions on the ground plane, and we can use image elements. To find mutual impedance we calculate the reaction integral over the surface of one element, with an assumed current distribution, times the field radiated from the first antenna. The first antenna and its image radiate to the second antenna. Since the reaction integral is over the surface of the second antenna, its image is not included in the integral. The elements along the

edge can have a different pattern than the central elements, and a full moment method solution accounts for differing current distributions. The next approximation assumes that the antenna elements radiate in fundamental modes with fixed current distributions. For example, these could be sinusoidal current distributions on dipoles that reduce the basis functions to one on each antenna.

Because we have a linear problem, we can calculate the coupling (or mutual impedance) between elements using pairs. Assuming only one mode on each antenna reduces the matrix problem to one with rank equal to the number of elements. We multiply the inverse impedance matrix by the excitation voltage vector to find the current on each element (one mode on each). This method becomes intractable for a large array, because we must invert the impedance matrix.

The next level of approximation assumes that all antennas are surrounded by the same element configuration. We assume that the edge elements have the same effective pattern as the inner elements. If we supply power to one element, its radiation is received by all other elements in the array that excites currents on the element simply as a scaled version of the fundamental mode. For this analysis we feed only a single element and calculate the current excited on nearby elements loaded by their characteristic impedance. This suggests an experimental approach of feeding a single element surrounded by other loaded elements. We call this the *array element pattern* or *scan element pattern* (formally the *active element pattern*). Analytically, we calculate the mutual impedance matrix and add twice the element resistance to the diagonal elements to account for the loop of source and load resistance on the antennas. We invert this matrix and find the current on the fed element and on its loaded nearby neighbors. This current sum radiates a pattern that we associate with the fed element and call it the array element pattern. We assume that all elements radiate the same pattern and multiply by the array factor to calculate the array pattern.

Consider an array of V-dipoles mounted on a ground plane. To equalize the E- and H-plane beamwidths, we tilt the elements 30° toward the ground plane. This broadens the E-plane beamwidth by removing the pattern null along the horizontal plane due to the dipole current. We reduce the mutual coupling when we locate a horizontal dipole over a ground plane because its image radiation decreases the radiated field of antenna along the ground plane. Figure 12-14 plots the E-plane pattern of the V-dipole tilted 30° when located in a hexagon array of loaded elements for 2 (19) and 3 (37) rings of elements. The radiation from currents excited on the extra dipoles widens the pattern beamwidth and lowers gain. The H-plane pattern (Figure 12-15) has lower gain than the isolated element, but narrower beamwidth. The increased E-plane beamwidth has decreased gain and the H-plane narrowed beamwidth fails to offset the gain loss significantly. The analysis shows the increased pattern ripple as more elements are added. These plots illustrate results expected from calculations or measurements on an antenna element where the ground plane reduced mutual coupling.

Figure 12-16 gives the pattern of an edge element in the V-dipole array in the E-plane. The analysis placed the elements over an infinite ground plane to eliminate ground-plane effects. We see significant asymmetry in the pattern due to its placement. Of course, we expect a large variation from this small array for the edge element. As we increase array size, these effects diminish. It is reasonable to start with an idealized element pattern for the initial design since array element pattern effects are small for good elements. As the design progresses an array element pattern should be measured (or calculated) and used for analysis at the next level.

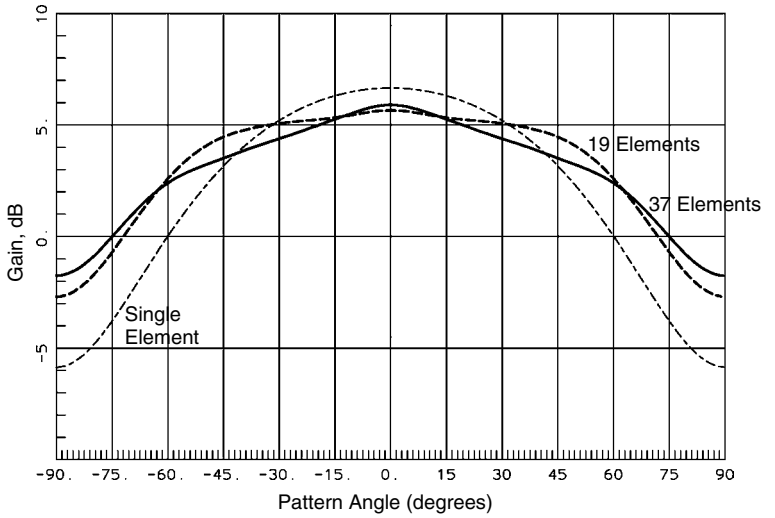

FIGURE 12-14 *E*-plane pattern of a V-dipole tilted 30° located in the center of a hexagon array.

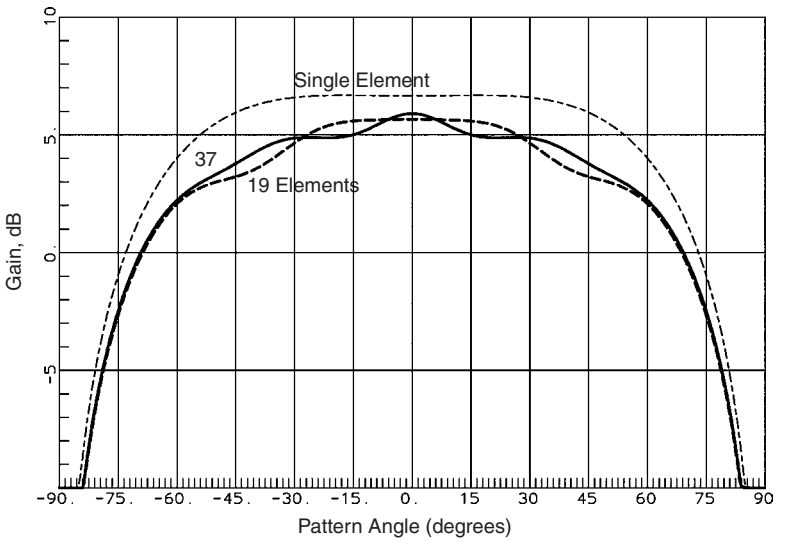

FIGURE 12-15 *H*-plane pattern of a V-dipole tilted 30° located in the center of a hexagon array.

12-6 FEED NETWORKS

12-6.1 Corporate Feed

Figures 12-17 and 12-18 illustrate schematically the two types of constrained feeds. In these networks we route signals through transmission lines and power dividers to deliver power to each element for transmittal and, by reciprocity, route the receive signals to single outputs. A phase shifter is placed between the power division network and every antenna element to scan the beam. The corporate feeds in Figure 12-17

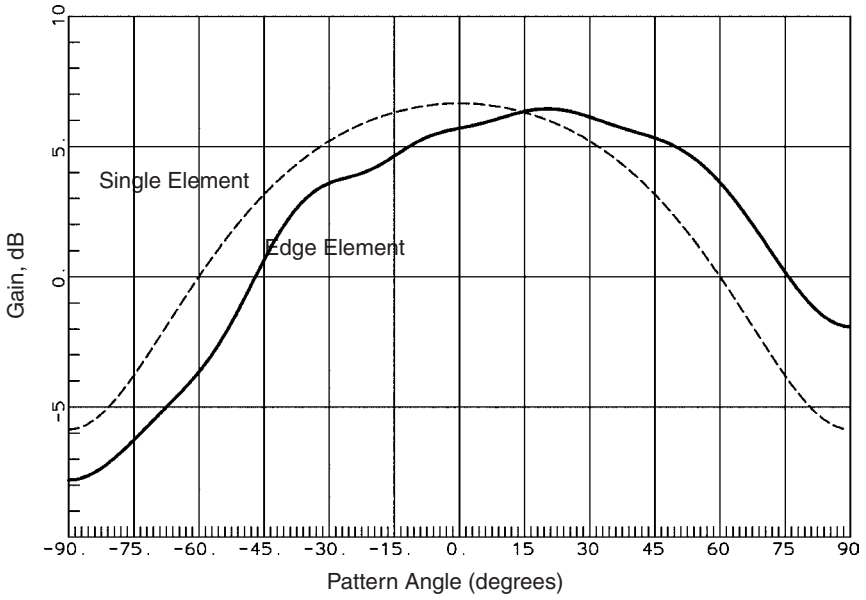

FIGURE 12-16 *E*-plane pattern of a V-dipole tilted 30° located at the edge of a hexagon array.

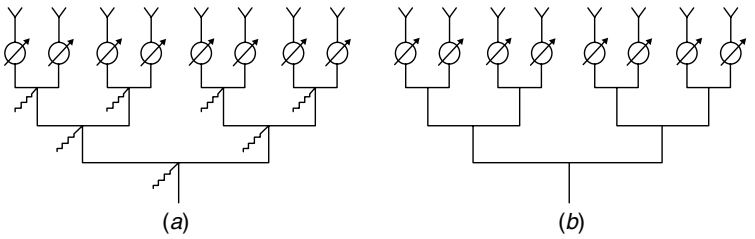

FIGURE 12-17 Corporate feeds: (*a*) matched with isolation resistors; (*b*) reactive. (From T. C. Cheston and J. Frank, Array antennas, Chapter 11 in M. I. Skolnik, ed., *Radar Handbook,* Fig. 38, © 1990 McGraw-Hill.)

usually divide to 2^N elements because two-way power dividers have the simplest designs. The matched corporate feed contains isolation resistors on the power dividers. We fabricate power dividers from four-port microwave circuits where one port is isolated, which means that in normal matched-impedance operation it receives no signal. When the output ports do not have matched loads, a portion of the reflected signal will be dissipated in the load on the isolated port. The impedance of phased array elements change as we scan the beam and it is impossible to match the elements at all scan angles. The isolation resistors prevent propagation of these reflected signals beyond the first network, whereas reactive power divider networks cannot prevent the accumulation of errors as the phase array scans. These networks work best in fixed-beam operation, not in phased arrays. Isolation resistors dissipate no power under impedance-matched conditions. In Section 11-7 we discuss how to analyze the connection between the feed network and the array with its mutual coupling, to calculate the resulting feed coefficients of the array.

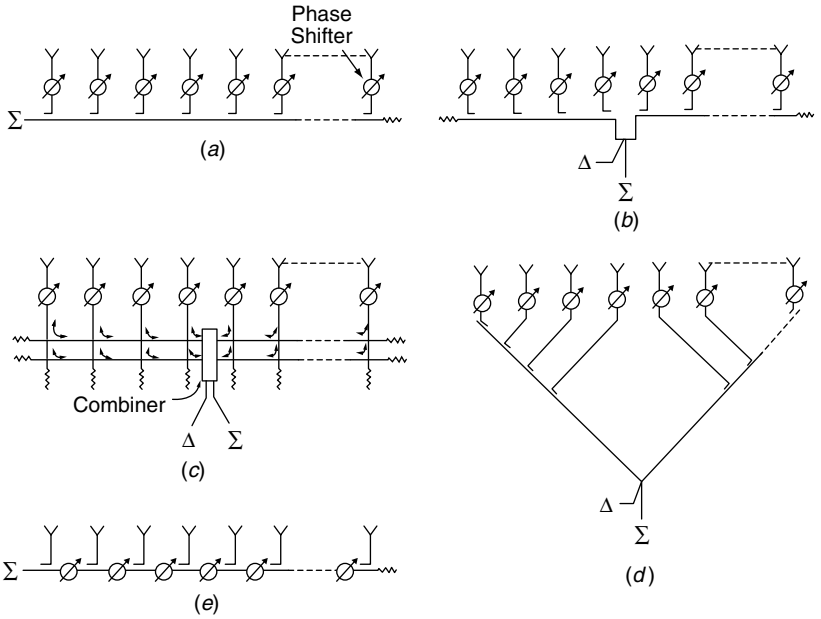

FIGURE 12-18 Series feed networks: (*a*) end feed; (*b*) center feed; (*c*) center feed with separately optimized sum and difference channels; (*d*) equal-path-length feed; (*e*) series phase shifters. (From T. C. Cheston and J. Frank, Array antennas, Chapter 11 in M. I. Skolnik, ed., *Radar Handbook,* Fig. 37, © 1990 McGraw-Hill.)

12-6.2 Series Feed

Figure 12-18 shows types of series feeds. We use series feeds for frequency scanning, but these contain phase shifters that can scan the beam in other directions not determined by frequency scanning. Of course, a series feed has limited bandwidth because the long transmission lines cause frequency scanning. The end feed in Figure 12-18*a* is the same as the waveguide-fed slot array, which has a bandwidth $50\%/N$, where N is the number of elements along the line. Feeding in the center, Figure 12-18*b* doubles the bandwidth and allows both sum and difference feeding used in monopulse. The network of Figure 12-18*c* has separate lines for sum and difference distributions so that each can be optimized. This double line configuration does suffer from coupling between the two rows of couplers because of the limited isolation in the couplers and the changing impedance as the array scans. If we place the phase shifters along the feeder line as shown in Figure 12-18*e*, all can be set to the same value to scan the beam. The problem is that each phase shifter has loss and these accumulate as the signal travels down the feed line. The network in Figure 12-18*a* has the loss of only one phase shifter. By equalizing the path lengths in each arm (Figure 12-18*d*), we increase the frequency bandwidth to that of the phase shifters and array size, because series feed frequency scanning is eliminated.

12-6.3 Variable Power Divider and Phase Shifter

Figure 12-19 gives the schematic of two transmission-line couplers connected in tandem with lines that contain phase shifters. We build 3-dB power divider couplers in stripline made with a centerboard with totally overlapped lines a quarter-wavelength

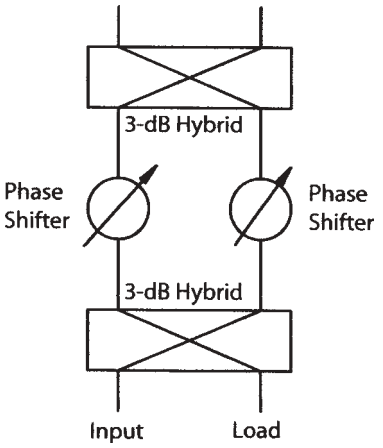

FIGURE 12-19 Variable power divider and phase shifter combination.

long in the dielectric. In a dielectric of 2.21 the centerboard is 0.013 in. (0.33 mm) thick and the outer spacers to the two ground planes are 0.062 in. (1.60 mm) thick. The totally overlapped lines are 0.065 in. (1.65 mm) wide to produce a 3-dB coupler. By crossing over the two coupled lines, the outputs occur on the side opposite the feed.

If the phase shifters have the same value, the network produces a 0-dB coupler where signals at the left input flow to the right output. Of course, the network has symmetry, and a signal at the right input couples totally to the left output. Through the two couplers the signal switches from one side of the centerboard to the other side. This dual coupler can be used to cross signals in a feed network without using the vertical vias that are useful for the construction of Butler matrices and other feed networks where crossovers are needed.

With two phase shifters in the lines between the two couplers, as shown in Figure 12-19, we can build a combination variable power divider and phase shifter. The voltage coupling c_p is determined by the phase difference in the two paths:

$$\phi_2 - \phi_1 = \cos^{-1}(1 - 2c_p^2) \tag{12-24}$$

The output phase of the two arms is given by

$$\text{phase} = \phi_1 - \tan^{-1}\frac{\sin(\phi_2 - \phi_1)}{1 - \cos(\phi_2 - \phi_1)} \tag{12-25}$$

Figure 12-20 shows a feed network using variable power dividers so that the output can be any amplitude and phase distribution. We discussed the formation of multiple beams from a single input in Section 3-6. We can form any combination of beams when we have control of both amplitude and phase. Of course, the array size limits our ability to form distinct beams, but the beamwidth of each beam is determined by the full size of the array. Each power divider is variable. Since the output from a variable power divider with one phase shifter can be any amplitude, we only need the extra phase shifter, either in the last variable power divider or on the output as shown. Because the network provides one input, the gain drops as we form multiple beams. No power is lost in the loads for impedance-matched outputs. Depending on

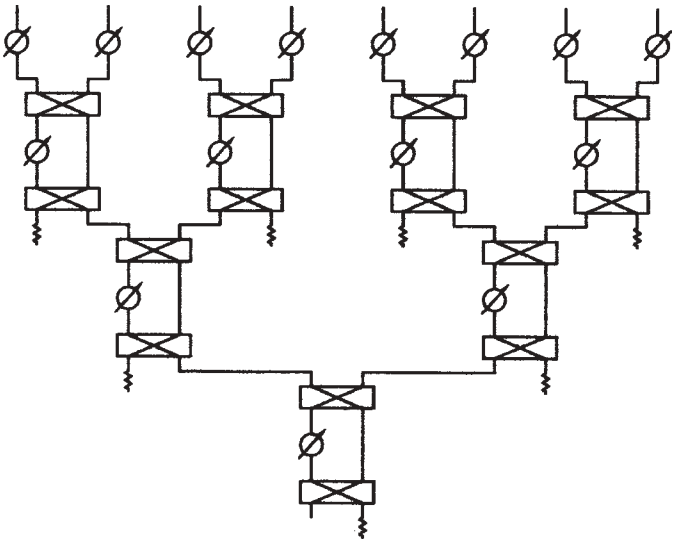

FIGURE 12-20 Eight-element feed network using variable power dividers with final phase shifters at the elements.

the phase of the outputs, the reflected signals from the antennas are either dissipated in the isolation loads or appear at the input.

12-6.4 Butler Matrix [9]

A Butler matrix is a feed network with 2^N inputs and 2^N outputs used to feed a uniformly spaced line array that produces a beam for every input port. The network consists of 3-dB hybrid couplers and fixed phase shifters. Figure 12-21 shows the schematic of the microwave feed network for eight ports. Each input port produces a uniform-amplitude distribution on the outputs with a uniform phase slope across the ports. We can use 0-dB couplers for the internal line crossings because adding couplers to an etching for the centerboard of a stripline has no cost. We make the output line crossings by using equal-length coaxial lines connecting the feed network to the antennas.

Each input port of the Butler matrix has the full gain of the array. On transmit we provide 2^N inputs and insert 2^N times the power of a single input into the feed network that provides full power to each beam. If we scan an array to an angle different from the angle of the input wave, the array will either dissipate the signal in internal loads or scatter it, but it does not collect at the input port. A Butler matrix provides an input port for the sequence of waves incident from 2^N directions. Signals from these directions are not dissipated or scattered, but the array collects them with the full gain of the array.

Figure 12-22 plots the patterns for all eight ports of a Butler matrix feeding an array with $\lambda/2$-element spacing. The array elements have 90° beamwidths and the further scanned patterns show the decrease due to element pattern. The uniform-amplitude arrays radiate 13.2-dB sidelobes, which limits the separation of the signals into the various input ports. The pattern peaks occur at evenly spaced values of u-space, where

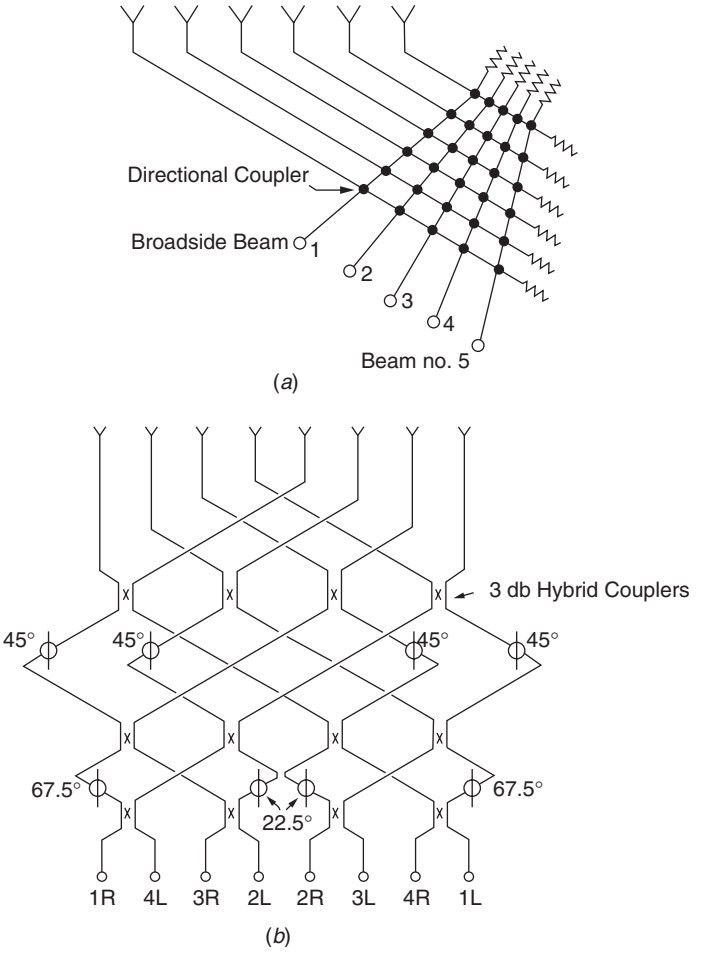

FIGURE 12-21 Eight-element Butler matrix network: (*a*) equal-path-length beam-forming matrix; (*b*) eight-element, eight-beam matrix. (From T. C. Cheston and J. Frank, Array antennas, Chapter 11 in M. I. Skolnik, ed., *Radar Handbook,* Fig. 57, © 1990 McGraw-Hill.)

$u_i = (d/\lambda)(\sin\theta - \sin\theta_i)$ for an element spacing of d:

$$\sin\theta_i = \pm\frac{i\lambda}{2Nd} \qquad i = 1, 3, 5, \ldots, N-1 \tag{12-26}$$

The uniform amplitude line array has a pattern:

$$\frac{E_e(\theta)\sin N\pi u_i}{N\sin\pi u_i}$$

Since the minimum value of the index i is 1, the first beams scan from broadside. The crossover level between beams occurs at -3.92 dB for an isotropic element pattern.

Equation (12-26) shows that the beams move closer together as we increase the electrical distance between elements. Figure 12-23 gives the pattern response of a

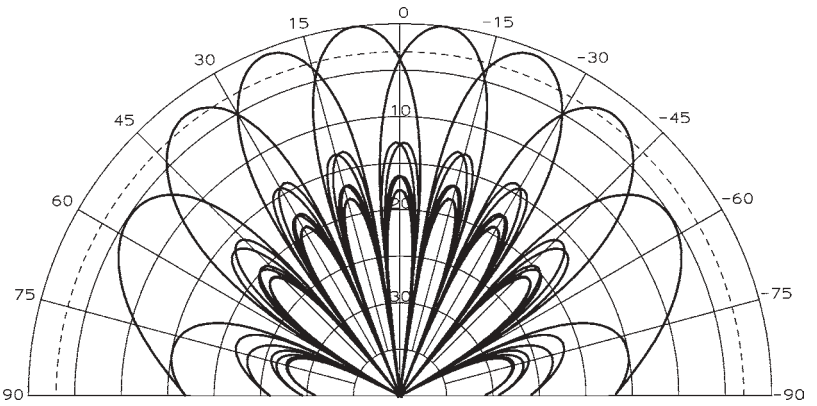

FIGURE 12-22 Patterns of an eight-element line array spaced λ/2 with Butler matrix feed.

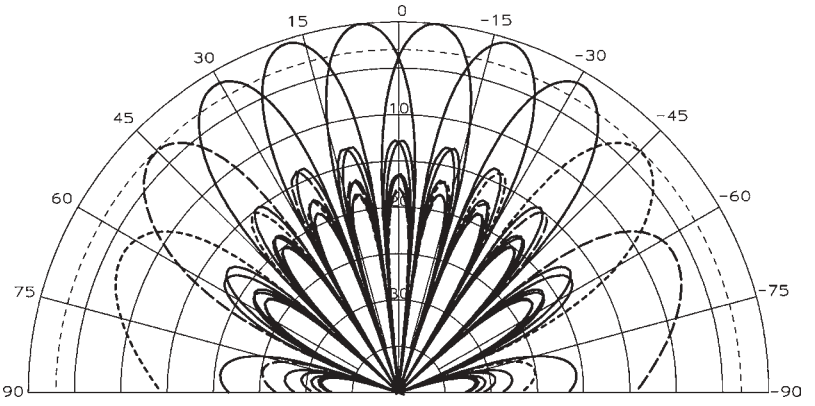

FIGURE 12-23 Patterns of an eight-element line array spaced 0.6λ with Butler matrix feed.

Butler matrix feeding an array with 0.6λ element spacing. All beams shift toward broadside. The crossover level is still at −3.92 dB and the first sidelobe level at 13.2 dB. The two dashed patterns radiate grating lobes reduced in amplitude only by the element pattern. The response seems to have 10 beams. Although the Butler matrix can be designed to cover an octave bandwidth by using quarter-wavelength hybrid couplers and compensated line Schiffman phase shifters [10], an array will not operate over this bandwidth without forming grating lobes. An octave-bandwidth Butler matrix is useful as the beamformer for a multiple-mode spiral antenna (Section 11-5.4).

12-6.5 Space Feeding

Instead of using a feed network with the signals constrained in transmission lines, we can use a feed antenna and an array of receiving antennas to distribute the signal. Figure 12-24 illustrates space feeding where a single feed antenna radiates to the backside of an array, where pickup antennas collect the signal and deliver it to a phase shifter and amplifier chain that feed the radiating antennas of the array. Of course, this feeding method can be used for reception as well. Although Figure 12-24 shows a line array, we actually have a planar array.

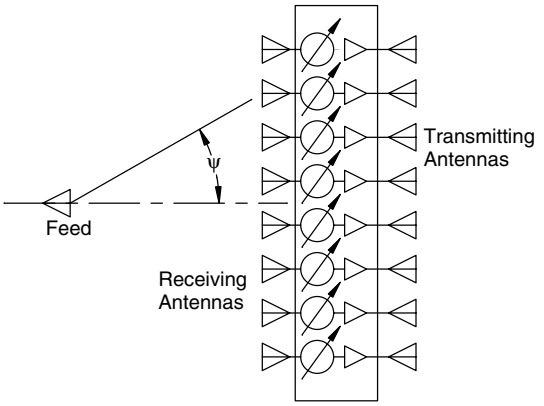

FIGURE 12-24 Space-fed array.

We analyze this feed network as a lens. The phase shifters compensate for the phase shift due to the extra transmission distance and eliminate the quadratic phase error, but the network cannot compensate for the amplitude taper. The feed-antenna-narrowed beamwidth, which matches the angular extent of the plane to reduce spillover loss, reduces amplitude to the edge elements. Similarly, the receiving antennas have a pattern that adds to the amplitude taper. We equate feed power in differential area to aperture power in a differential area [Eq. (9-11)]:

$$\frac{A(r,\phi)}{F(\psi,\phi)} = \frac{\sin\psi}{r}\frac{d\psi}{dr}$$

We add the geometry of the flat-plate receiving surface and carry out the indicated operations to find the distribution on the array:

$$A(r,\phi) = \frac{F(\psi,\phi)R(\psi,\phi)\cos^3\psi}{f^2} \tag{12-27}$$

Equation (12-27) includes a receive antenna power pattern $R(\psi,\phi)$. Of course, the feed arrangement can be offset instead of centrally fed as shown, with phase shifters compensating for the different feed path lengths.

12-6.6 Tapered Feed Network with Uniform-Amplitude Subarrays

One approach to produce a wider bandwidth array is to combine a feed network containing time-delay networks that feed subarrays. We construct the subarrays with identical networks containing phase shifters and a uniform-amplitude distribution. We apply the amplitude taper to the smaller feed array that feeds the subarrays to lower sidelobes. The beam scanned with time-delay networks does not shift when frequency changes, but the phase shifters cause phase stepping across the array face. This causes quantization lobes.

Initially, we consider the array at broadside, where it does not matter whether the input feed network contains time-delay networks or phase shifters. We consider the subarray to be the element pattern of the smaller input feed network. Figure 12-25 shows the pattern at broadside using an eight-element subarray and a 16-element input array that zero-sampled a linear 30-dB Taylor distribution ($\overline{n} = 6$). Because the

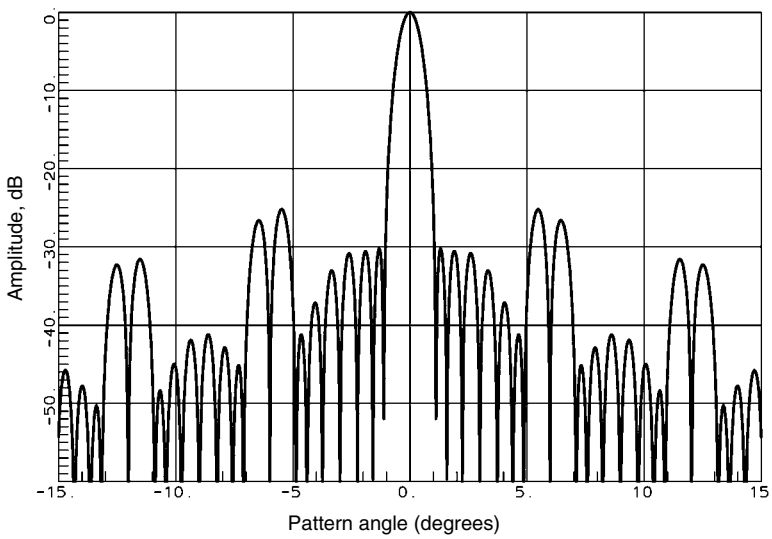

FIGURE 12-25 Paired sidelobes of a 128-element array with a 16-element subarray with an eight-element 30-dB Taylor distribution feed network.

sidelobes of the uniform array do not occur at the same angles as the Taylor distribution, Figure 12-25 contains paired high sidelobes. Decreasing the number of elements in the feed array to eight causes the paired sidelobes to rise above 30 dB because the distribution controls only seven nulls instead of the 15 shown in Figure 12-25.

When we scan the beam, we apply phase shift to both feed and subarray so that the beams remain aligned. This presents no pattern problem if we use continuous phase shifters, but when we quantize the phase shifters, misalignment occurs unless we space elements on $\lambda/2$ centers. Figure 12-26 gives the pattern responses a for 128-element

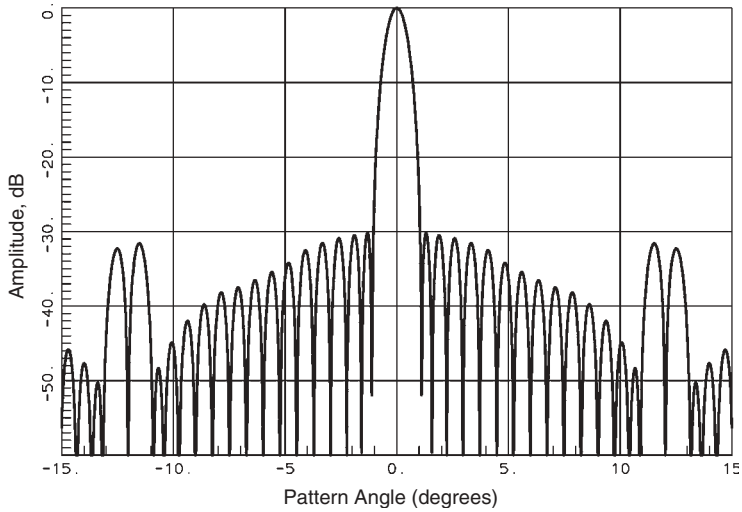

FIGURE 12-26 Paired sidelobes of a 128-element array with an eight-element subarray with a 16-element 30-dB Taylor distribution feed network.

array with an eight-element uniform-amplitude subarray and a 16-element feed array with a 30-dB Taylor ($\overline{n} = 6$) sampled distribution for 0.6λ element spacing. The curve occurs when the feed array has 4-bit phase shifters and the feed array has 3-bit phase shifters. Decreasing the feed array to 3 bits or reducing the number of elements degrades the sidelobes further. Adding time-delay networks does not eliminate these problems because the subarray and feed network sidelobes increase their misalignment when frequency shifts even for elements initially on $\lambda/2$ centers.

The solution to these problems lies in using an overlapped subarray scheme [11]. In this case we need multiple inputs to the feed array, such as a Butler matrix, whose outputs feed multiple subarrays. One method uses space feeding so that all Butler matrix output ports feed every subarray. We phase the multiple input ports in a Woodward synthesis (Section 4-8) to form a flat-top pattern output for the subarray. The flat-top pattern eliminates the misalignment between the subarray and feed patterns and allows the use of time-delay networks. The overlapped subarray method greatly complicates the feed network.

12-7 PATTERN NULL FORMATION IN ARBITRARY ARRAY

In Chapter 4 we discussed the control of an array pattern by manipulation of pattern nulls. In Section 4-9 we applied the Schelkunoff unit-circle method to line arrays. In Sections 4-21 and 4-22 we combined nulls found for rhombic and linear arrays to synthesize planar arrays by convolution. We can extend these ideas to arbitrarily positioned and oriented arrays. We start with the equation for the pattern for any array with feed coefficients w_n:

$$\mathbf{E}(\theta, \phi) = \sum_{n=1}^{N} [E_{\theta n}(\theta, \phi)\hat{\theta} + E_{\phi n}(\theta, \phi)\hat{\phi}] w_n e^{j\mathbf{k}\cdot\mathbf{r_n}} \tag{12-28}$$

The array elements can be oriented arbitrarily and located at $\mathbf{r}_n = (x_n, y_n, z_n)$ with the vector propagation constant $\mathbf{k} = k(\sin\theta\cos\phi, \sin\theta\sin\phi, \cos\theta)$. We calculate the pattern for one element of the array in a particular direction $\mathbf{k}_m = k(\sin\theta_m\cos\phi_m, \sin\theta_m \sin\phi_m, \cos\theta_m)$:

$$\mathbf{S}_{m,n} = [E_{\theta n}(\theta_m, \phi_m)\hat{\theta} + E_{\phi n}(\theta_m, \phi_m)\hat{\phi}] e^{j\mathbf{k}_m\cdot\mathbf{r_n}} \tag{12-29}$$

The array pattern in direction m is found by combining Eqs. (12-28) and (12-29):

$$\mathbf{E}_m(\theta_m, \phi_m) = \sum_{n=1}^{N} \mathbf{S}_{m,n} w_n \tag{12-30}$$

Since we only have one set of coefficients, w_n, only a single linear combination of the theta and phi components can form a null in a given direction. We project the polarization components of each element onto a particular polarization that reduces Eq. (12-29) to a single scalar term. For a given direction we define the vector $[\mathbf{S}_{i,n}]$ using patterns of the array elements in direction $\mathbf{k}_i$ evaluated projected on a given polarization:

$$[\mathbf{S}_{i,n}] = [S_{i,1}, S_{i,2}, \ldots, S_{i,N}]^{\mathrm{T}} \tag{12-31}$$

The operation $[\cdot]^{\mathrm{T}}$ is the matrix transpose and $[\mathbf{S}_{i,n}]$ is a column vector.

We start with an initial vector $[w_0]$ of array feeding coefficients that includes amplitudes and phases. We modify the coefficients to form a pattern null $\mathbf{k}_1 = k(\sin\theta_1\cos\phi_1, \sin\theta_1\sin\phi_1, \cos\theta_1)$ by multiplying the coefficient vector by a matrix found from the pattern of each element in that direction:

$$[w_p] = \left\{\mathbf{I} - \frac{[S_{1,n}]^*[S_{1,n}]^{\mathrm{T}}}{[S_{1,n}]^{\mathrm{T}}[S_{1,n}]^*}\right\}[w_0] = \left\{\mathbf{I} - \frac{[S_{1,n}]^*[S_{1,n}]^{\mathrm{T}}}{A}\right\}[w_0] = [P_1][w_0] \quad (12\text{-}32)$$

The product of the column vector and its transform generates an $n \times n$ matrix. The coefficient A is a summation: $A = \sum_{n=1}^{N} S_{1,n}S_{1,n}^*$. Equation (12-32) is derived from Gram–Schmidt vector orthogonalization [12, pp. 41–46]. The vector $[w_0]$ is the initial state of the array that includes any amplitude distribution to lower sidelobes and the phasing to scan the beam. We form nulls after scanning the beam.

This process can be extended to multiple nulls, but numerical precision and the number of elements limit the process and it is exact only for the last null. Equation (12-32) extends to m ($< N - 1$) nulls by matrix multiplication:

$$[w_p] = [P_m]\cdots[P_2][P_1][w_0] \quad (12\text{-}33)$$

The method does not exactly match the locations of initial nulls, but it improves when we have large arrays. We do not need to store the matrix $[P_i]$ because its elements are easily formed from the vector $[S_{i,n}]$ when needed, and by starting with $[w_0]$ we work Eq. (12-33) from right to left and store the new excitation vector at each step.

To design an array we specify $N - 1$ nulls and one desired signal direction. We extend Eq. (12-30) to a matrix for a given beam direction $E_1(\theta_1, \phi_1)$ and the direction of $N - 1$ nulls:

$$\begin{bmatrix} E_1(\theta_1,\phi_1) \\ E_2(\theta_2,\phi_2) \\ \vdots \\ E_N(\theta_N,\phi_N) \end{bmatrix} = \begin{bmatrix} S_{1,1} & S_{1,2} & \cdots & S_{1,N} \\ S_{2,1} & S_{2,2} & \cdots & S_{2,N} \\ \vdots & \vdots & \ddots & \vdots \\ S_{N,1} & S_{N,2} & \cdots & S_{N,N} \end{bmatrix} \begin{bmatrix} w_1 \\ w_2 \\ \vdots \\ w_N \end{bmatrix} \quad (12\text{-}34)$$

We invert the matrix to find the feeding coefficients:

$$\begin{bmatrix} w_1 \\ w_2 \\ \vdots \\ w_N \end{bmatrix} = \begin{bmatrix} S_{1,1} & S_{1,2} & \cdots & S_{1,N} \\ S_{2,1} & S_{2,2} & \cdots & S_{2,N} \\ \vdots & \vdots & \ddots & \vdots \\ S_{N,1} & S_{N,2} & \cdots & S_{N,N} \end{bmatrix}^{-1} \begin{bmatrix} E_1(\theta_1,\phi_1) \\ E_2(\theta_2,\phi_2) \\ \vdots \\ E_N(\theta_N,\phi_N) \end{bmatrix} \quad (12\text{-}35)$$

All N coefficients of the vector E are not necessarily zero, we could solve for multiple beams with individually specified levels. The array has N degrees of freedom. This analysis ignores the effects of mutual coupling, whereas scattering from nearby objects can be included in the element patterns because this development has not assumed identical array elements. We can use the results of Section 3-11 to compensate the network for mutual coupling, but this development leads to an adaptive array which changes its feeding coefficients based on incident fields.

12-8 PHASED ARRAY APPLICATION TO COMMUNICATION SYSTEMS

Radar has been the chief application of phased arrays, but small arrays find application in communication systems. Terrestrial line-of-sight (LOS) microwave systems use multiple antennas to reduce downtime due to fading, but these systems operate at very high connectivity. Cellular telephone operates with high multipath that produces a Rayleigh probability distribution because most of the time there is no direct signal path (Section 1-19). Diversity combining improves connectivity in the same manner as the LOS system by providing an alternative path when the signal fades in the first path. The LOS system has slowly varying fades due to changing atmospheric conditions, while cellular telephone has rapid fades as the user moves. Diversity combining reduces signal null depths but does little to increase the average signal.

The second cellular telephone system problem is channel capacity. The number of users continues to grow and their demand for service soon saturates existing systems. Adding phase arrays to base stations provides multiple beams to subdivide the cells that allow improvements without building new sites. Beyond using fixed multiple beams formed by networks such as Butler matrices, adaptive arrays (*smart antennas*) increase capacity. Antennas are the same pieces of metal; adaptive electronic beamforming is the smart part. Since adaptive array analysis and design are mostly signal processing, they will not be discussed in detail.

When signals fade in one channel because the user or a scattering object moves, a second signal uncorrelated to the cause of the fade may provide a better communication path. If we have two signals, it may be better to combine them to reduce fading. We discuss two signals, and the extension to more is straightforward. Imagine two antennas and a network that connects them. The best system uses *maximal ratio combining* (MRC), which adjusts both amplitude and phase (complex phasers) of the two signals before adding them. MRC requires the most complicated equipment, because we need a variable power divider combined with a phase shifter. *Equal gain combining* (EGC) is a phased array with only a phase shifter that brings both signals to a common phase before combining them. *Selective combining* (SEC) detects the strongest signal and switches to it and ignores the second signal. Finally, we have *switch combining* (SWC), which switches when the signal drops below a threshold. Of course, SWC can switch back and forth rapidly when the signal drops in both paths. SWC is the lowest-cost system because it needs only one receiver front end.

A communication system provides connectivity at a given probability and we accept dropped calls and lost data. Fortunately, voice encoding can tolerate high BER (bit error rate), whereas LOS systems use error detection and retransmit to lower errors to near zero. Diversity gain measures the increased signal level at a given probability at the average signal level. Propagation models give us the log-normal (median) signal level, about which the level varies rapidly due to multipath. Diversity gain is usually given relative to the 90% signal reliability level, the improvement that allows a lower median signal level. We relate the improvement to the difference in signal level in the two channels Δ (dB) and the branch correlation ρ. Branch correlation measures the independence between the two signals. For example, polarization separation is one method to generate two channels, and cross-polarization in the two channels produces signal correlation. In other implementations two antennas are separated either vertically or horizontally, so a fade in reception at one antenna has a minor effect on the other. Two channels that receive the same signal have $\rho = 1$, whereas the ideal two-channel

system has $\rho = 0$. The following diversity gain (dB) at the 90% signal reliability level has been found empirically for the various combining techniques [13, p. 48]:

$$\text{Gain (dB)} = \begin{cases} 7.14e^{-0.59\rho}e^{-0.11\Delta} & \text{MRC} \\ -8.98 + 15.22e^{-0.2\rho}e^{-0.04\Delta} & \text{EGC} \\ 5.71e^{-0.87\rho}e^{-0.16\Delta} & \text{SEC} \end{cases} \tag{12-36}$$

MRC always produces a positive diversity gain. Selecting the larger signal has less benefit than MRC, and the EGC system can actually give a negative diversity gain under unfavorable situations. If the signal drops in one channel, adding two signals reduces overall performance because in essence the high signal level channel is reduced by 3 dB by the power divider.

Adaptive arrays (smart antennas) improve the system by directing a main beam at a particular user while producing nulls in directions of interfering signals. These signals could be from nearby cells using the same frequencies. Adaptive receiving arrays enable closer frequency reuse between cells and increases system capacity while improving quality of transmission. We either adaptively control element excitation at RF or detect and combine them at IF. The weak link in the cellular telephone system is the transmission from the mobile to the base station, and the base station contains the array used to separate signals, so we concentrate on the receiving path.

The array either uses the least mean squares (LMS) algorithm or an eigen-decomposition technique to set the element weights. LMS requires a known reference signal on which the system minimizes the errors. This system adjusts the weights to maximize the S/N ratio. The known signal can be a portion of the coded waveform transmitted by the mobile unit, which increases overhead and reduces transmit rate slightly when each unit sends a unique reference signal. The LMS algorithm can adjust weights to optimize the constant amplitude of receive signal, since a phased modulated wave (PSK, QPSK) has constant amplitude. Systems that optimize on a known reference signal include recursive least squares and Wiener filter methods.

Eigen-decomposition techniques operate without a known reference signal. A cross-correlation matrix is formed from the input signals by considering their locations using the terms of Eq. (12-29). A cross-correlation matrix is the product of the pairs of these terms using the complex conjugate of one factor. By solving the eigenvalue problem, the algorithm detects directions of incoming signals and the beamforming is based on the angular information of these beams. Two commonly used algorithms are MUSIC and ESPRIT.

To increase system performance significantly, we use digital beamforming, where we connect a receiver to every antenna. We can make as many copies of the signals after detection and form the beams digitally without loss of S/N. We had to detect the signals anyway to apply the adaptive array algorithms that set the element weights at RF. Digital beamforming eliminates the phase shifters and variable power dividers on the antennas and replaces them with receiver components. Element location and quantization values of the receiver components still affect the array patterns, but by using adaptive algorithms, enable production of identical arrays. The array adjusts to its location and the input signals by using signal processing—a smart antenna.

12-9 NEAR-FIELD MEASUREMENTS ON PHASED ARRAYS

Near-field measurements produce excellent diagnostics of phased arrays. We exercise the phase shifters and measure element outputs directly. Initially we built small loop

probes and moved them across the array face and recorded measurements. The small probes have little effect on the array elements, due to mutual coupling, because they are poor antennas. We improve precision by fabricating scanners to hold and position the probes at the array elements. Unfortunately, if we move the probe away from the array surface to reduce the probe effect on the elements, increased signal is received from more than one array element and it is difficult to separate element responses. The answer lies in using the transforms of near-field measurements to separate element responses.

Figure 12-27 shows the simulated response of radiation to a 90° beamwidth probe positioned directly over a 64-element linear array made with 90° beamwidth elements. The array sampled a 30-dB Taylor linear aperture distribution to set its amplitudes, and the twentieth element amplitude was reduced by 6 dB. The two dashed curves give the responses at $\lambda/2$ and 3λ above the surface. The probe located at $\lambda/2$ produces a response with about a 3-dB dip at the twentieth element. The probe at 3λ above the array face gives a vague dip over a number of elements. Both probe heights measure responses with significant ripples. Many arrays have been measured and corrected using this approach.

A planar near-field measurement combined with simple mathematical transforms produces better results. We scan the near-field probe sufficiently above the array to reduce mutual coupling effects that change what we are measuring. Planar near-field measurements take readings at evenly spaced intervals and use the fast Fourier transform (FFT) to calculate the far-field response at points evenly spaced in $\sin\theta$-space, where θ is measured from the planar normal. The planar measurements use $k_x = \sin\theta_x = \sin\theta\cos\phi$ and $k_y = \sin\theta_y = \sin\theta\sin\phi$ found from an FFT along each axis. For example, we transform each row along the x-axis using the FFT algorithm and transform resulting columns of FFT on the rows along the y-axis. The FFT requires 2^N samples along the array face and produces the same number of pattern directions

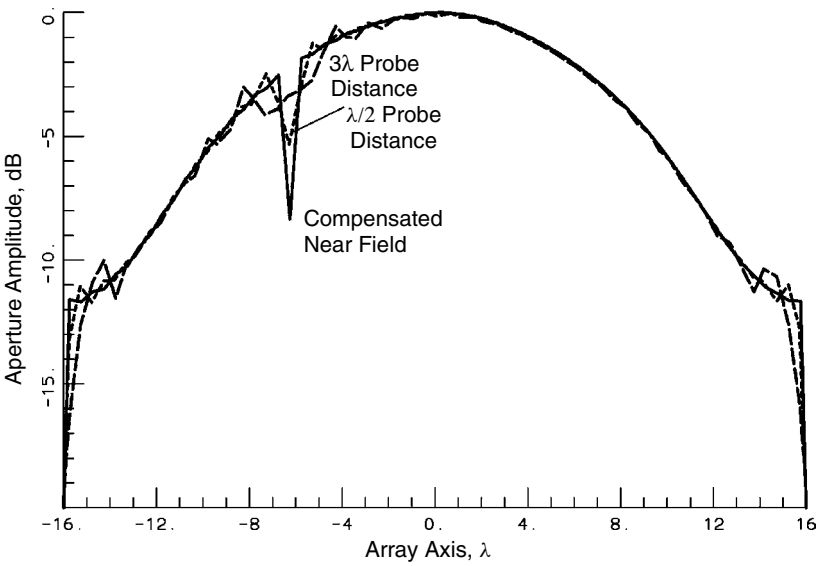

FIGURE 12-27 Near field measurements of a 64-element line array with 30-dB Taylor distribution at probe distances of 3λ, $\lambda/2$, and compensated to face.

TABLE 12-5 Planar Near-Field Sampling to a Far-Field Pattern Using FFT

Aperture Spacing, d (λ)	Sin θ_{max}	θ_{max} (deg)
0.25	2	Invisible space
0.5	1	90
0.75	2/3	41.8
1.0	0.5	30
2.0	0.25	14.48

evenly spaced in $\sin\theta$-space. We find the range of k_x-space from the aperture sampling spacing d:

$$\sin\theta_{max} = \pm\frac{\lambda}{2d} \tag{12-37}$$

Table 12-5 shows that sampling closer than $\lambda/2$ produces pattern points in invisible space, and for most arrays, larger sampling spacing fails to produce a point over each element. Since we want to capture the radiation from the edge elements, it is necessary to scan the near-field probe beyond the edge of the array face. If we space the probe a distance a above the array space, we should sample out to the maximum transformed angle. Given an array of length D and probe length L, the maximum angle for accurate measurements is given by $\theta_c = \tan^{-1}[(L - D)/(2a)]$. If we use $\lambda/2$ sampling distance, L extends to ∞ and we compromise by also assuming that the array element beamwidth captures most of the power radiated. After probing the field, we transform to the far field by using FFT^{-1}. This pattern has been multiplied by the probe antenna pattern and the pattern of a Huygens source (Section 2-2) of an aperture. The Huygens source has a pattern $E_H(\theta) = \cos^2(\theta/2)$. The far-field pattern also has a phase distribution relative to the array face, due to the distance between the face and the probe plane a distance a above it. We apply probe compensation and shift the far-field phase so that when we transform the k-space pattern back to the aperture, the scan plane lies on the array face. Given the desired position z for the new aperture plane, we first adjust the far-field pattern:

$$E_{new}(\theta_x, \theta_y) = \frac{E(\theta_x, \theta_y)e^{-jk\cos\theta_x(z-a)}e^{-jk\cos\theta_y(z-a)}}{E_{probe}(\theta_x, \theta_y)\cos^2(\theta_x/2)\cos^2(\theta_y/2)} \tag{12-38}$$

The solid curve on Figure 12-29 shows the results of these calculations on the array with altered element amplitude when $z = 0$. If the array contained more feeding errors, all of them would appear in the FFT of the far field to the near-field aperture plane. We use the same method to determine errors in paraboloidal reflectors, but we apply multiple steps to the z-axis plane position in the back transform to produce planar cross sections through the reflector surface.

REFERENCES

1. H. A. Wheeler, The radiation resistance of an antenna in an infinite array or waveguide, *Proceedings of IRE*, vol. 36, April 1948, pp. 478–488.

2. H. A. Wheeler, Simple relations derived from a phased-array antenna made of an infinite current sheet, *IEEE Transactions on Antennas and Propagation*, vol. AP-13, no. 4, July 1965, pp. 506–514.
3. R. C. Hansen, Linear arrays, Chapter 9 in A. W. Rudge et al., eds., *Handbook of Antenna Design*, IEE/Peter Peregrinus, London, 1983.
4. M. I. Skolnik, Nonuniform arrays, Chapter 6 in R. E. Collin and F. J. Zucker, eds., *Antenna Theory*, Part 2, McGraw-Hill, New York, 1969.
5. R. J. Mailloux, Periodic arrays, Chapter 13 in Y. T. Lo and S. W. Lee, eds., *Antenna Handbook*, Van Nostrand Reinhold, New York, 1992.
6. R. J. Mailloux, *Phase Array Antenna Handbook*, Artech House, Boston, 1994, pp. 393–399.
7. T. A. Milligan, Space tapered circular (ring) arrays, *IEEE Antennas and Propagation Magazine*, vol. 46, no. 3, June 2004.
8. M. I. Skolnik, J. W. Sherman III, and F. C. Ogg, Jr., Statistically designed density tapered arrays, *IEEE Transactions on Antennas and Propagation*, vol. AP-12, no. 4, July 1964, pp. 408–417.
9. J. L. Butler, Digital, matrix, and intermediate-frequency scanning, in R. C. Hansen, ed., *Microwave Scanning Antennas*, Vol. III, Academic Press, New York, 1966.
10. B. M. Schiffman, A new class of broadband microwave 90° phase shifters, *IRE Transactions on Microwave Theory and Techniques*, Vol. MTT-6, no. 4, April 1958, pp. 232–237.
11. R. Tang, Survey of time-delay beam steering techniques, *1970 Phased Array Conference*, Artech House, Boston, 1972.
12. J. E. Hudson, *Adaptive Array Principles*, IEE/Peter Peregrinus, Stevenage, Hertfordshire, England, 1981.
13. A. Paulraj et al., Space-time processing in wireless communications, *Proceedings of the 3rd Workshop on Smart Antennas in Wireless Mobile Communications*, Stanford University, Stanford, CA, 1996.